THE JOURNAL OF PHYSICAL CHEMISTRY C

Article

pubs.acs.org/JPCC

Effects of Water Adsorption and Surface Oxidation on the Electrical Conductivity of Silicon Nanocrystal Films

Neema Rastgar,[†] David J. Rowe,[‡] Rebecca J. Anthony,[‡] Brian A. Merritt,[†] Uwe R. Kortshagen,[‡] and Eray S. Aydil*[,†]

[†]Department of Chemical Engineering and Materials Science, University of Minnesota, 421 Washington Ave SE, Minneapolis, Minnesota 55455, United States

[‡]Department of Mechanical Engineering, University of Minnesota, 111 Church Street SE, Minneapolis, Minnesota 55455, United States

ABSTRACT: Electrical conductivities of thin films of silicon nanocrystals (4−6 nm) exhibit high sensitivity to water vapor. Specifically, water adsorption on the surface of silicon nanocrystals films increases their electrical conductivity by a factor of 4 at room temperature and an order of magnitude at 175 K. The increase in conductivity is reversible and can manifest as peaks or hysteresis loops in temperature-dependent conductivity measurements even when the measurements are conducted under vacuum at 10^{-5} Torr and in the presence of only residual amounts of water vapor. Hydrogen-terminated silicon nanocrystals are easily oxidized to form submonolayer to a monolayer of chemically bound oxygen on their surfaces when annealed at 300 °C in a glovebox with 0.1 ppm of water vapor. Annealing under vacuum at 300 °C retains H-passivation without oxidation. The electrical conductivity of films made from hydrogen-terminated silicon nanocrystals is 200 times higher than the electrical conductivity of films made from silicon nanocrystals with a monolayer of chemically bound oxygen. However, the conductivities of both types of films increase upon adsorption of water on the nanocrystal surfaces. These findings underscore the importance of controlling silicon nanocrystal surfaces in determining the electrical properties of their thin films.

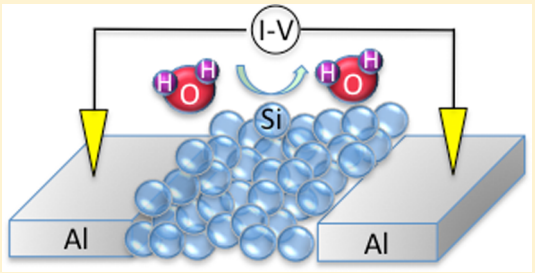

INTRODUCTION

Semiconductor nanocrystals (NCs) are under consideration for potential applications in optoelectronic devices such as solar cells[1−3] and light-emitting diodes[4−6] because they are inexpensive and solution processable and their properties can be tuned by changing their size. Silicon NCs are particularly promising because they are earth-abundant and nontoxic. Moreover, controllable doping in Si NCs has recently been achieved.[7] Many applications require charge carrier transport in NC films. For Si NC films, charge transport mechanisms are typically studied through electrical conductivity measurements,[8,9] often as a function of temperature. However, such measurements can be affected by oxidation and adsorption of gas molecules on the nanocrystal surfaces.[10] Here, we report the effects of water vapor adsorption and surface oxidation on the electrical conductivity of Si NC films.

EXPERIMENTAL METHODS

Silicon NCs were synthesized in a capacitively coupled nonthermal radio-frequency plasma through electron impact dissociation of silane gas diluted with argon.[11] The NC size was controlled by changing the NC residence time within the plasma. The NC diameters used in this study were between 4 and 6 nm. Some of the films were deposited from NCs that were exposed to hydrogen gas injected into the afterglow of the SiH_4/Ar plasma. The surfaces of as-synthesized NCs are hydrogen-terminated,[12,13] and additional hydrogen injection into the plasma afterglow has been shown to improve hydrogen surface coverage and reduce the surface defect density.[14] Nanocrystal films (100−500 nm thick) were deposited downstream of the plasma via ballistic aerosol impaction[15,16] on glass substrates that were prepatterned with electron-beam-evaporated interdigitated aluminum electrodes (Figure 1a). The effective electrode width for 100 μm digit spacing is 13.1 mm. Ballistic aerosol impaction was achieved by supersonic expansion of the gas carrying the NCs through a rectangular nozzle aimed at the substrate. A top-down scanning electron microscopy (SEM) image of a NC film is shown in Figure 1b, where the aluminum electrode edges are outlined.

Following deposition, films were annealed at 300 °C for 1 h, either on a hot plate inside a nitrogen glovebox or on a heated substrate holder in a vacuum chamber at 5×10^{-6} Torr. The films were transferred directly from the reactor to the glovebox in a vacuum suitcase without coming into contact with ambient air, whereas the films annealed in the vacuum chamber were exposed to ambient air for a few seconds during the transfer. FTIR spectra do not show oxidation during this brief exposure or during vacuum annealing (*vide infra*). Oxygen and water

Received: August 20, 2012
Revised: December 13, 2012
Published: February 4, 2013

   dx.doi.org/10.1021/jp308279m | *J. Phys. Chem. C* 2013, 117, 4211−4218

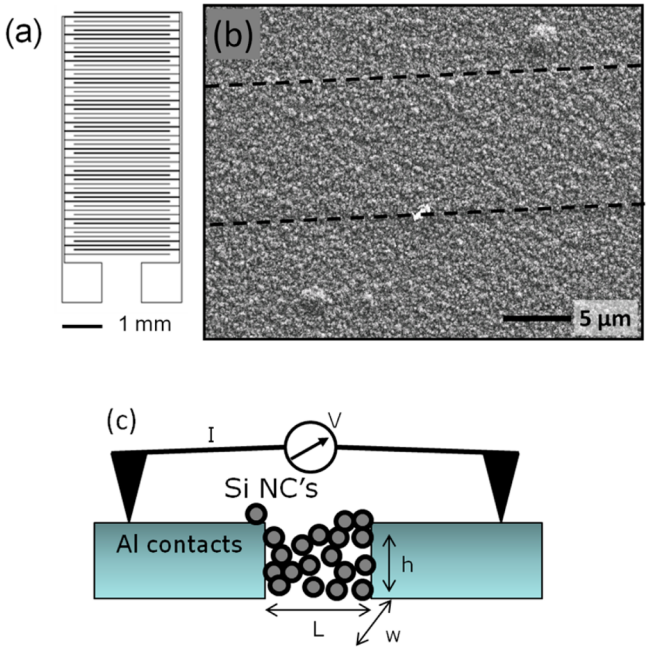

Figure 1. (a) Top-view diagram of the aluminum interdigitated contacts. Spacing between horizontal digits is 100 μm, and the total effective width of each contact is 13.1 mm. (b) Top-view SEM of a Si NC film deposited on and in between two aluminum digits via aerosol impaction after plasma synthesis. The dashed lines show the edges of the aluminum contacts beneath the nanocrystal film. (c) Two-point probe geometry used to measure the electrical characteristics of the silicon NC films.

levels inside the glovebox were 10 and 0.1 ppm, respectively. Film annealing has previously been shown to improve the conductivity of Si NC films.[17] Before any annealing (in vacuum or in glovebox), the films and contacts were too resistive for measurements. Attenuated total reflectance Fourier transform infrared (ATR-FTIR) spectra were collected from NC films deposited onto ZnSe crystals before and after annealing to determine any changes to the NC surfaces. These ATR-FTIR measurements were conducted in a vacuum chamber equipped with a Nicolet Magna-IR 550 spectrometer and described in detail in previous publications.[18,19]

Electrical conductivities of the NC films were measured between 360 and 135 K in a Janis variable temperature vacuum cryostat using an Agilent 4155C Semiconductor Parameter Analyzer. The base pressure of the cryostat was 10^{-5} Torr. The NC film temperature was controlled through resistive heating or cooling of the sample stage inside the cryostat. Sample temperature was measured using a platinum wire-bound resistance temperature detector (Omega, RTD) placed directly on top of the substrate. Current–voltage characteristics were recorded using the simple two-point probe geometry shown in Figure 1c. The current passing through the film was measured while the applied voltage was swept from 0 to 40 V, typically in 1 V increments. Conductivity was also measured during deliberate exposure of the cryostat atmosphere to water vapor or dry argon gas at or above room temperature. Finally, residual gases were detected using a quadrupole mass spectrometer (Extorr XT300) attached downstream of the chamber housing the cryostat.

RESULTS AND DISCUSSION

Effect of Water Adsorption on Conductivity. Figure 2a shows the linear and log–log current–voltage (I–V) character-

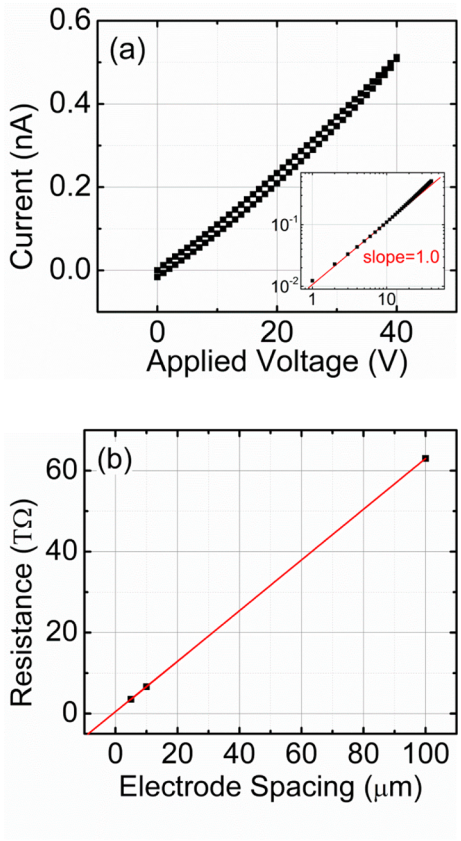

Figure 2. (a) Linear and log–log current–voltage characteristics of a silicon NC film measured at room temperature. This particular film was annealed at 300 °C and was 500 nm thick. (b) Resistance versus electrode separation for a Si NC film.

istics of a Si NC film at room temperature and 10^{-5} Torr. The I–V characteristics were Ohmic (see Figure 2a, inset), and the film conductivity was determined from the slope of the I–V characteristics,[20] the film thickness, and the dimensions of the interdigitated electrodes. We surmise that the slight hysteresis observed in the I–V characteristics is due to charging of the film through trapping. The contact resistance was small compared to the Si NC film resistance as evidenced by Figure 2b, which shows the measured resistance as a function of electrode spacing. The measured resistance extrapolates to an intercept that is negligible compared to the measured resistances, and resistance versus electrode spacing goes nearly through the origin.

Figure 3 shows the current measured through a Si NC film at 40 V as a function of time as the film is exposed to water vapor. Two data sets in the figure represent similar measurements performed at room temperature and at 330 K. The experiment begins at time t = 0 with the NC film in the vacuum chamber at a base pressure of 10^{-5} Torr. At t = 20 min, water vapor from a bulb filled with liquid water is admitted to the chamber through a needle valve. At steady state, the pressure in the vacuum chamber reaches 4 mTorr, and almost all of this pressure is due to water vapor in the chamber. After 15 h, the needle valve is closed, and the chamber is evacuated to 10^{-5} Torr.

dx.doi.org/10.1021/jp308279m | J. Phys. Chem. C 2013, 117, 4211–4218

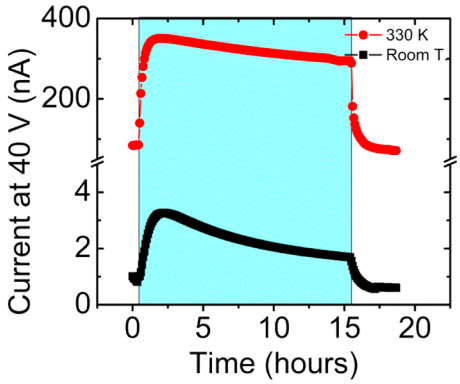

Figure 3. Current through a Si NC film at 40 V as a function of time at room temperature (bottom, black) and 330 K (top, red). The shaded region (blue) indicates NC film exposure to 4 mTorr of water vapor.

Measurements at room temperature and at 330 K both show the same trend when NCs are exposed to water vapor (depicted by the blue shaded region). The NC film conductivity increases approximately by a factor of 4 and reaches a steady state. This increase in conductivity appears to be caused by adsorption of water on the NC surfaces. During the next 15 h, while a constant (4 mTorr) water vapor pressure is maintained over the NC film, the film conductivity decreases by ~20% at 330 K and by ~50% at room temperature. We attribute this decrease to slow oxidation of the NC surfaces as the adsorbed water reacts with Si. Gradual oxidation of NC surfaces has previously been observed in ambient air.[21] When the water vapor flow is turned off and the water vapor pressure over the NC film is reduced, the film conductivity decreases with a time constant of ≈60 and ≈90 min at 330 K and room temperature, respectively. The reversibility of the increase in film conductivity is strong evidence that this increase is due to physical adsorption of water on the Si NCs.

The final steady-state conductivity of the NC film at 10^{-5} Torr after stopping water exposure is lower by ~15% at 330 K and by 35% at room temperature than the initial value at $t = 0$. This irreversible decrease in conductivity upon 15 h of water exposure is attributed to slow irreversible oxidation of the NC surface during water exposure. Thus, we identify two effects of water exposure on the NC film conductivity: a reversible increase in conductivity due to water exposure and an irreversible decrease due to slow oxidation of the NC surface.

Temperature Dependence of Conductivity. Figure 4a shows the conductivity of a Si NC film as a function of temperature. Several factors combine to determine the complicated temperature dependence of the Si NC film conductivity. First, the conductivity of a semiconductor NC film is expected to decrease with decreasing temperature and is typically given by $\sigma = \sigma_0 \exp(T_0/T)^m$, where m depends on the conduction mechanism.[22] For example, $m = 1$, $m = 1/2$, and $m = 1/4$ correspond to charge transport with Arrhenius activation, Efros-Shklovskii, and Mott variable-range hopping mechanisms, respectively. Different conduction mechanisms may dominate in different temperature regimes. When the data in Figure 4a are analyzed by plotting ln σ vs T^{-m}, none of these models produce a line over the entire temperature range. Moreover, the dependence of the conductivity on temperature is too strong to be explained by Efros-Shklovskii and Mott variable-range hopping. It is therefore likely that the temperature dependence is due to an activated process in the NC film though the

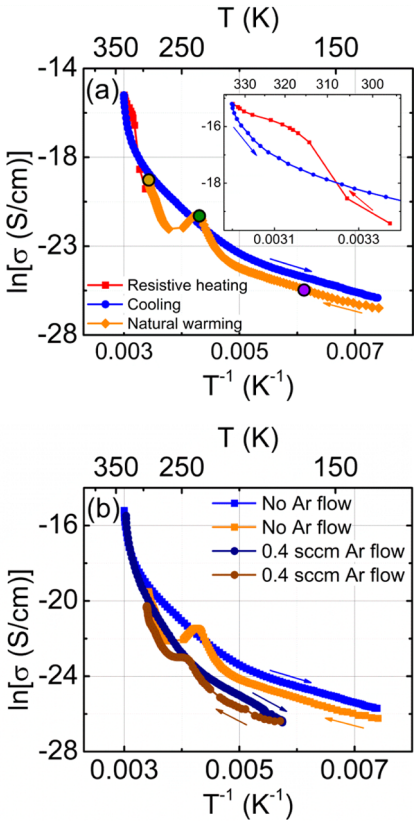

Figure 4. (a) NC film electrical conductivity as a function of temperature while heating the film from room temperature to 330 K (red squares), while cooling the film to 135 K (blue circles), and while warming the film from 135 K to room temperature (orange diamonds). The inset is an expanded view of the region between 300 and 330 K. (b) NC film conductivity as a function of temperature (a) with 0.4 sccm dry argon flow through the chamber (navy and brown circles). The experiment in (b) was otherwise identical to that in (a), and the data from (a) are replotted in (b) for comparison.

interpretation of the data in Figure 4a is significantly complicated by the effects of water adsorption and desorption on NC surfaces during the measurement.

The sensitivity of the NC film conductivity to the water adsorption and to the presence of residual water vapor in the chamber (even at 10^{-5} Torr) introduces hysteresis in temperature-dependent conductivity measurements and complicates their interpretation. For example, in the particular experiment shown in Figure 4a, the NC film was first heated from room temperature to 330 K (red), then cooled to 135 K (blue), and allowed to warm back up to room temperature (orange). The conductivity of the NC film increases monotonically when the film is heated from room temperature to 330 K and decreases monotonically as the film is cooled to 135 K. Below 135 K, the film becomes too insulating, and the current falls below the noise level of the Semiconductor Parameter Analyzer. During this measurement, conductivity versus temperature exhibits hysteresis. Specifically, the conductivity measured while heating the NC film from ~310 to ~330 K is higher than that measured during cooling from ~330 to ~310 K (Figure 4a, inset), and the conductivity measured while cooling from ~310 to ~135 K is higher than that measured during heating the NC film from ~135 K to room temperature. Surprisingly, a clear peak in conductivity versus temperature is

dx.doi.org/10.1021/jp308279m | J. Phys. Chem. C 2013, 117, 4211−4218

also observed at ~235 K during heating from ~135 K to room temperature.

The hysteresis and nonmonotonic behavior in the conductivity versus temperature are due to changes in the residual water vapor pressure in the chamber. The presence of residual water vapor in high vacuum is inevitable. As the temperature of the cryostat is decreased, residual water vapor adsorbs on the cryostat platen and on the chamber walls, and the water vapor pressure in the chamber decreases. Conversely, when the cryostat and the chamber walls are heated, water molecules desorb from the walls, and the residual water vapor pressure in the chamber rises. These changes in water vapor pressure as a function of cryostat temperature affect the conductivity of the NC film as shown in the controlled experiments in Figure 2. The changes in the residual water vapor pressure with cryostat temperature are illustrated in Figure 5, which shows the mass

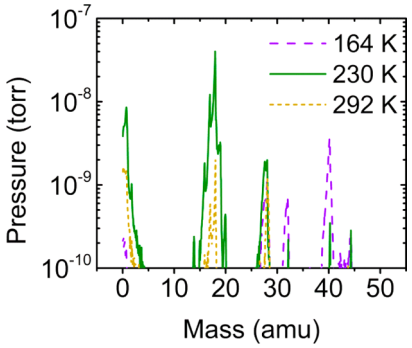

Figure 5. Mass spectra of residual gases in the chamber collected at three different temperatures shown with circles in Figure 4a.

spectra of residual gases in the cryostat chamber at three different temperatures marked by circles in Figure 4a. These spectra were taken during heating from 135 K to room temperature. At 164 K, residual water vapor is not detected because all water is condensed on cold surfaces, including the NCs. As the cryostat and the chamber surfaces are heated, water begins to desorb at ~220 K and reaches a maximum at ~235 K.[23]

We now explain the changes in conductivity during the experiment shown in Figure 4a. When the heater is turned on to heat the NC film from room temperature to 330 K, the water adsorbed on the walls of the chamber near the heating element desorbs and increases the water vapor partial pressure in the vacuum chamber. The water adsorbs onto the colder NC surfaces and increases conductivity. This increase is in addition to an increase due to thermal activation alone during heating to 330 K and explains why the slope of the resistive heating curve is initially steep; the slope here is affected by both thermal carrier activation as well as water adsorption. As the substrate temperature rises, however, water desorbs from the NC surfaces. Moreover, the water vapor desorbed from the chamber walls during heating is pumped away, and the water vapor pressure in the chamber decreases. Consequently, the slope of the conductivity versus temperature measurement during heating begins to decrease near 330 K. During cooling, residual water vapor in the cryostat atmosphere rapidly condenses on the chamber walls near the liquid nitrogen reservoir. This reduces the partial pressure of water vapor in the chamber, and conductivity decreases steeply upon initiating the liquid nitrogen flow to cool the substrate to 135 K.

At 135 K, water is adsorbed to the NC surface and all walls and surfaces inside the chamber. Once the liquid nitrogen flow is turned off, the substrate as well as the entire chamber begins to warm toward room temperature. During warming from 135 K to room temperature, the conductivity initially parallels the conductivity measured during cooling. The chamber walls are at somewhat elevated temperatures compared to the NC film. As the chamber begins to warm, water condensed on the walls desorbs and increases the partial pressure of water vapor in the chamber. This burst of water then adsorbs onto the colder film and accelerates the increases in conductivity at 220 K. This is the reason for the increase in slope before the peak at ~235 K. Residual gas analysis data shown in Figure 5 confirms this burst of water: water peaks at 16−18 amu increase significantly at 230 K compared to the levels at 292 and 164 K. Previous temperature-programmed desorption studies have found that molecular water desorbs from Si surfaces at ~225 K.[23] As the NC film temperature increases from 235 K, water begins to desorb from NC film surfaces and the film's electrical conductivity decreases. Moreover, the water that had desorbed from the film surfaces is pumped out of the system. These factors all contribute to a subsequent decrease in the conductivity even as the substrate temperature is increased, causing the peak shown in conductivity at ~235 K.

The experiment in Figure 4a was repeated while flowing 0.4 sccm of dry argon gas over the NC film, and the conductivity vs temperature data acquired during this experiment are shown in Figure 4b. The goal was to provide dry inert gas flow during the measurement to reduce the water vapor pressure in the chamber and sweep out any water desorbing from the walls. Indeed above 315 K, the two cooling conductivity curves (blue and navy) now match closely, and the hysteresis as well as the magnitude of the peak at 235 K is reduced significantly. The data from Figure 4a (during cooling) are replotted in Figure 4b for comparison. As expected, the experiment with dry argon flow produces lower conductivities than the experiment without dry argon flow. For example, at 175 K, the conductivity of the film measured with dry argon flow is approximately an order of magnitude lower than that without argon flow. Dry argon flow through the vacuum chamber reduces water adsorption on the NC film by sweeping water vapor from the chamber and reducing the water partial pressure.

Infrared Spectroscopy of the NC Surfaces. Given the importance of the surfaces in determining the NC film conductivity, we examined the surfaces of the NCs using ATR-FTIR. Figure 6 shows the ATR-FTIR spectrum of a Si NC film deposited on a ZnSe ATR crystal with hydrogen injection into the afterglow region of the plasma, as well as the spectra of these NC films after annealing in a nitrogen glovebox and after annealing in vacuum. All spectra are with respect to a bare ZnSe ATR crystal. The as-synthesized film exhibits two strong peaks (labeled 2 and 3) at 2131 and 2106 cm^{-1}, corresponding closely to surface $Si-Si-H_3$ and symmetric Si_2-Si-H_2 hydride stretching modes, respectively.[24] The presence of wagging mode absorptions at 908 and 859 cm^{-1} (not shown) confirms that the surface is primarily terminated with silicon di- and trihydrides. The shoulder at ~2073 cm^{-1} (labeled 1) also indicates the presence of monohydrides. There are no absorptions in the 2180−2280 cm^{-1} range, which would indicate the presence of oxygen-backbonded silicon hydrides ($O_{4-x}-Si-H_x$).[25,26] After annealing in vacuum, a 22% decrease in the trihydride peak intensity is observed, while the dihydride peak intensity decays only by 4%. The loss of surface

dx.doi.org/10.1021/jp308279m | J. Phys. Chem. C 2013, 117, 4211−4218

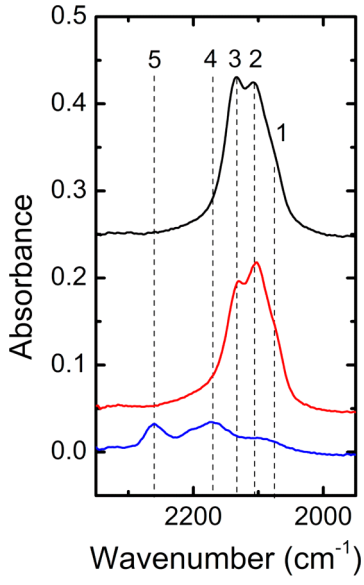

Figure 6. ATR-FTIR spectra (with respect to a bare ZnSe ATR crystal) of a Si NC film synthesized with postplasma hydrogen injection before annealing (top, black), after annealing in vacuum (middle, red), and after annealing in a glovebox (bottom, blue) both at 300 °C. Peak 1: 2073 cm^{-1}; peak 2: 2106 cm^{-1}; peak 3: 2131 cm^{-1}; peak 4: 2171 cm^{-1}; peak 5: 2262 cm^{-1}.

trihydrides before dihydrides with increasing temperature has been reported previously for silicon nanoparticles.[27] After annealing in a nitrogen glovebox, the absorption at 2131, 2106, and 2073 cm^{-1} are reduced dramatically. Three broad absorptions at 2262, 2206, and 2171 cm^{-1} appear and are assigned to surface mono-, di-, and trihydride Si−H stretching modes where the Si atoms are backbonded to oxygen atoms.[26,28,29] In addition, a large, broad peak between 1250 and 950 cm^{-1} (not shown) also appears, indicating the presence of Si−O−Si bonds. These results suggest that glovebox annealing Si NC films at 300 °C for 1 h oxidizes NC surfaces, while vacuum annealing under the same time and temperature conditions does little to change the surface coverage of the as-synthesized films.

Conductivity of Films with Unoxidized NCs. The electrical conductivity of NC films annealed under vacuum was found to be up to 200 times higher than films annealed in the glovebox. For example, Figure 7 compares the room-temperature $I-V$ characteristics of Si NC films annealed in the glovebox to $I-V$ characteristics of Si NC films annealed in vacuum. Both films were deposited from NCs synthesized with hydrogen injection in the afterglow region of the plasma. NC films annealed in vacuum remain H-terminated, and their surfaces are not oxidized, whereas NC films annealed in the glovebox have a very thin layer of H-terminated oxide (Figure 6). The oxide thickness is estimated to be 2 Å from the integrated area under the Si−O−Si peak between 1250 and 950 cm^{-1} (not shown).[26] This value is on the order of the Si−O bond length (1.6 Å), indicating a submonolayer or at most a monolayer of silicon oxide. In fact, O insertion in all surface Si atom backbonds would account for both the amount of oxide observed and the changes in the Si−H absorption spectra. Both films show Ohmic $I-V$ characteristics.

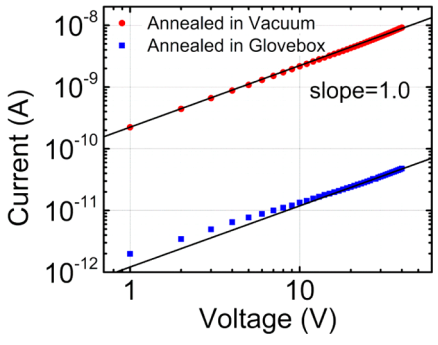

Figure 7. Log−log $I-V$ characteristics of a Si NC film annealed in glovebox (blue squares) and one annealed in vacuum (red circles), measured at room temperature. The lines represent slopes of 1.0.

Figure 8a compares the temperature dependence of the conductivity of Si NC films annealed in the glovebox to those annealed in vacuum. Conductivities were measured while cooling from room temperature to 260 K, where a noise limit of the measurement was reached, and again while heating from 260 K to room temperature. Arrows indicate the direction of the temperature sweep. The temperature-dependent conductivity data form a counterclockwise hysteresis loop for both films though the conductivity of the NC film annealed in vacuum is much higher than that of the NC film annealed in the glovebox. Figure 8b shows the effect of argon flow on the hysteresis for a NC film that was annealed in the glovebox. In this particular experiment, the measurement is started at 350 K where we believe the water adsorbed on the NCs is minimized. When the measurement is conducted without argon flow, the conductivities measured during heating are significantly higher than those measured during cooling. This difference is due to water vapor desorbing from the internal walls of the chamber and increasing the water vapor partial pressure above the NC film. Argon flow significantly diminishes the width of the hysteresis. During the entire cooling range, the argon flow has a minimal effect on the conductivity since water adsorbed on the NC surfaces has been minimized. During heating, the conductivities measured under argon flow are lower than those measured without argon flow and closer to the conductivities measured during cooling. This reduction in hysteresis is attributed to argon flow carrying the water desorbing from the internal chamber walls and reducing the water vapor partial pressure in the chamber. Figure 8c shows similar conductivity measurements on a NC film annealed in vacuum. In the absence of argon flow, the conductivity exhibits a significant peak during cooling. The increasing edge of the peak during cooling is attributed to water adsorption on the NC surface. Further decreases in temperature eventually overcomes this increase, giving rise to the peak. The subsequent warming of the film also results in a peak in conductivity. This time, the peak is due to water desorption from the walls and is similar to those in Figures 4b and 8b. The contrast between Figures 8b and 8c is particularly striking as water adsorption has a much larger effect on unoxidized NC films than on oxidized NC films. The conductivity of films with unoxidized Si NCs is much more sensitive to water adsorption than the conductivity of films with oxidized Si NCs. When the measurements are repeated with argon flow, the peak in conductivity is not observed during cooling and hysteresis is minimized. This type of temperature dependence was reproducible on two different films synthesized and annealed under the same conditions.

Discussion of Possible Conduction Mechanisms. Linear fits to ln σ vs T^{-1} near room temperature yield

dx.doi.org/10.1021/jp308279m | J. Phys. Chem. C 2013, 117, 4211−4218

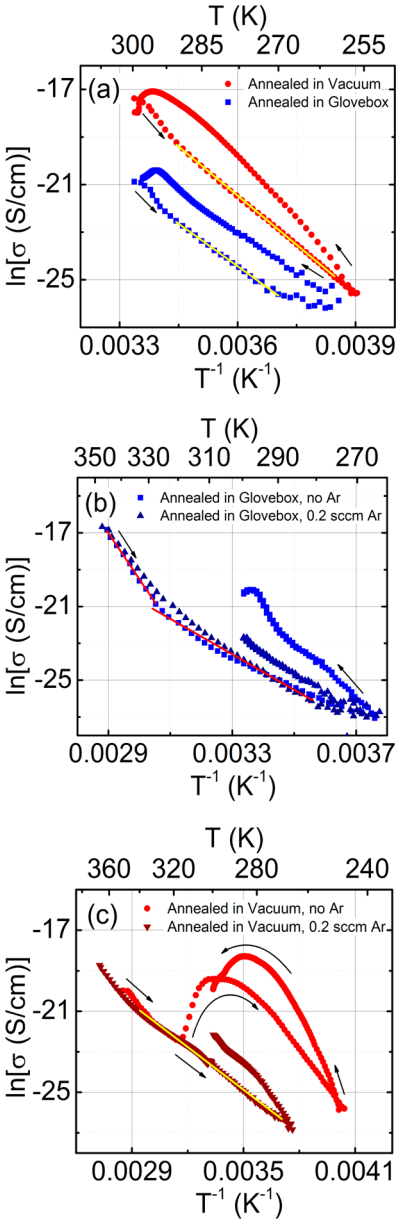

Figure 8. (a) Electrical conductivity of NC films annealed in vacuum or the glovebox as a function of temperature. The activation energy from the slopes (yellow lines) are 1 and 1.2 eV for the vacuum- and glovebox-annealed films, respectively. The effect of Ar flow on the electrical conductivity as a function of temperature for NC films (b) annealed in glovebox and (c) annealed in vacuum. In (b), the apparent activation energy extracted from the data between 325 and 350 K for the NC films annealed in the glovebox is 2.16 eV, whereas the apparent activation energy extracted from the data between 280 and 325 K for the same NCs is 0.83 eV (red lines). In (c) the apparent activation energy extracted from the data between 270 and 340 K is 0.6 eV (yellow line).

activation energy barriers significantly larger than half the band gap value expected for intrinsic activation of bulk Si or even for 4 nm diameter Si quantum dots with carrier confinement. Glovebox annealing forms a thin layer (approximately a monolayer) of oxide on the NC surfaces, which can act as a barrier to charge transport. Thus, the temperature dependence of conductivity shown in Figures 4, 8a, and 8b can be understood in terms of charge transport between Si NCs through a very thin oxidized layer. One mechanism by which charge can move from NC to NC is through successive thermionic emission across barriers between the NCs.[20] The large electron affinity and band gap difference between silicon oxide and Si NCs can present the charge with large barriers. A linear fit to the data for NC films annealed in the glovebox in Figure 8a between 290 and 260 K yields an activation energy of 1.2 eV, whereas a fit to the data for NC films annealed in vacuum between 290 and 270 K yields an activation energy of 1 eV. However, the slope of the ln σ vs T^{-1} changes significantly as a function of temperature for NC films annealed in the glovebox, perhaps indicating a distribution of barrier heights for thermionic emission. For example, the apparent activation energy extracted from the data between 325 and 350 K for the NC films annealed in the glovebox is 2.16 eV, whereas the apparent activation energy extracted from the data between 280 and 325 K for the same NCs is 0.83 eV (Figure 8b). This variation is less severe for films annealed under vacuum. For example, a single apparent activation energy of 0.6 eV can be extracted from the data between 270 and 340 K for films annealed in vacuum. The large variation in the slope with temperature in glovebox-annealed films can be rationalized in terms of an inhomogeneous space between the NCs characterized by inhomogeneous and differing degrees of oxidation. Such a situation is expected since the films are oxidized after the film has formed. The connections between the NCs can vary from unoxidized regions in close proximity of each other to regions where an oxide has formed. Dependence of barrier heights on oxide thickness is well-known in the metal oxide−semiconductor device literature,[30] and we attribute the inhomogeneity of the barrier heights to the inhomogeneity of NC oxidation.

The interpretation of the electrical transport data is significantly complicated by the effects of water adsorption. In general, water adsorption can affect the conductivity of semiconductors and oxides through ionic or electronic mechanisms.[31] Ionic mechanisms refer to current flowing by ionic conduction through a condensed and percolated liquid water layer on the surface of the NCs, as has been reported for porous silicon and silica gels.[32,33] Electronic mechanisms refer to conduction where adsorbed water affects film conductivity by injecting charge carriers into the semiconductor, passivating surface dangling bonds and releasing trapped charges, or changing the electric field at the NC surface and between the Si NCs. For example, Dubey et al. showed that water adsorption on 1 μm thick H-terminated n-type silicon films on oxide insulators increases the conductivity by inducing an accumulation of majority carriers near the surface.[34,35] Moreover, Dubey et al. showed conclusively that this effect is reversible and due to adsorbed water. For the Si NC films described here, water adsorption also improves conductivity reversibly and over a wide range of temperatures. If the conductivity enhancement was due to ionic conduction through a condensed and percolated liquid water phase, both the oxidized and unoxidized NC films should have had similar conductivities and similar sensitivities to water adsorption. This is not the case: H-terminated unoxidized films show significantly greater sensitivity to the effects of water adsorption than the oxidized NC films. Thus, we eliminate the possibility of ionic conduction and conclude that an electronic mechanism is entirely responsible for the increase in NC film conductivity upon water adsorption.

dx.doi.org/10.1021/jp308279m | J. Phys. Chem. C 2013, 117, 4211−4218

CONCLUSIONS

Electrical conductivities of H-terminated Si NC films are extremely sensitive to the presence of water vapor, even when the partial pressure of water vapor is as low as 10^{-5} Torr. Specifically, water adsorption on Si NC surfaces increases the film's conductivity by up to an order of magnitude. The increase is reversible, though prolonged exposure to water vapor (e.g., longer than 15 h at 1−10 mTorr of water vapor) can result in slow oxidation even at room temperature. Oxidation of the surface decreases the electrical conductivity of Si NC films irreversibly. The annealing environment is very important when processing Si NC thin films. The surfaces of the Si NCs can be oxidized even when they are annealed in 0.1 ppm levels of water. NC films annealed under vacuum ($<10^{-5}$ Torr) for less than 1 h at 300 °C remain H-terminated and can exhibit conductivities more than 2 orders of magnitude higher than films annealed in a glovebox with very low levels of water vapor.

AUTHOR INFORMATION

Corresponding Author

*E-mail aydil@umn.edu; phone (612)-625-8593.

Notes

The authors declare no competing financial interest.

ACKNOWLEDGMENTS

This work was supported primarily by the MRSEC Program of the National Science Foundation under Award DMR-0819885. R.J.A. and B.A.M. helped synthesize and characterize the NC films and were supported (R.J.A. partially) by the United States Department of Energy Office of Fusion Energy Science Contract DE-SC0001939. Parts of this work was carried out in the College of Science and Engineering Nanofabrication Center, which receives partial support from the NSF under the NNIN program, and in the Characterization Facility, which has received capital equipment funding from the NSF through the MRSEC program.

REFERENCES

(1) Kamat, P. V. Quantum Dot Solar Cells. Semiconductor Nanocrystals as Light Harvesters. *J. Phys. Chem. C* **2008**, *112*, 18737−18753.

(2) Anthony, R. J.; Cheng, K. Y.; Holman, Z. C.; Holmes, R. J.; Kortshagen, U. R. An All-Gas-Phase Approach for the Fabrication of Silicon Nanocrystal Light-Emitting Devices. *Nano Lett.* **2012**, *12*, 2822−2825.

(3) Liu, C.-Y.; Holman, Z. C.; Kortshagen, U. R. Optimization Si NC/P3HT Hybrid Solar Cells. *Adv. Funct. Mater.* **2010**, *20*, 2157−2164.

(4) Colvin, V. L.; Schlamp, M. C.; Alivisatos, A. P. Light Emitting Diodes Made from Cadmium Selenide Nanocrystals and a Semiconducting Polymer. *Nature* **1994**, *370*, 354−357.

(5) Coe, S.; Woo, K. W.; Bawendi, M.; Bulovic, V. Electroluminescence from Single Monolayers of Nanocrystals in Molecular Organic Devices. *Nature* **2002**, *420*, 800−803.

(6) Cheng, K.-Y.; Anthony, R.; Kortshagen, U. R.; Holmes, R. J. High Efficiency Silicon Nanocrystal Light-Emitting Devices. *Nano Lett.* **2011**, *11*, 1952−1956.

(7) Pi, X. D.; Gresback, R.; Liptak, R. W.; Campbell, S. A.; Kortshagen, U. Doping Efficiency, Dopant Location, and Oxidation of Si Nanocrystals. *Appl. Phys. Lett.* **2008**, *92*, 123102.

(8) Pereira, R. N.; Niesar, S.; You, W. B.; da Cunha, A. F.; Erhard, N.; Stegner, A. R.; Wiggers, H.; Willinger, M.-G.; Stutzmann, M.; Brandt, M. S. Solution Processed Network of Silicon Nanocrystals: The Role of Internanocrystal Medium on Semiconducting Behavior. *J. Phys. Chem. C* **2011**, *115*, 20120−20127.

(9) Stegner, A. R.; Pereira, R. N.; Klein, K.; Lechner, R.; Dietmueller, R.; Brandt, M. S.; Stutzmann, M.; Wiggers, H. Electronic Transport in Phosphorus Doped Silicon Nanocrystal Networks. *Phys. Rev. Lett.* **2008**, *100*, 026803.

(10) Leschkies, K. S.; Kang, M. S.; Aydil, E. S.; Norris, D. J. Influence of Atmospheric Gases on the Electrical Properties of PbSe Quantum-Dot Films. *J. Phys. Chem C* **2010**, *114*, 9988−9996.

(11) Mangolini, L.; Thimsen, E.; Kortshagen, U. High-Yield Plasma Synthesis of Luminescent Silicon Nanocrystals. *Nano Lett.* **2005**, *5*, 655−659.

(12) Mangolini, L.; Jurbergs, D.; Rogojina, E.; Kortshagen, U. Plasma Synthesis and Liquid-Phase Surface Passivation of Brightly Luminescent Si Nanocrystals. *J. Lumin.* **2006**, *3*, 3975−3978.

(13) Pi, X. D.; Mangolini, L.; Campbell, S. A.; Kortshagen, U. Room Temperature Atmospheric Oxidation of Silicon Nanocrystals after HF Etching. *Phys. Rev. B* **2007**, *75*, 085423.

(14) Anthony, R. J.; Rowe, D.; Stein, M.; Yang, J.; Kortshagen, U. Routes to Achieving High Quantum Yield Luminescence from Gas-Phase Produced Silicon Nanocrystals. *Adv. Funct. Mater.* **2011**, *21*, 4042−4046.

(15) Rao, N. P.; Tymiak, N.; Blum, J.; Neuman, A.; Lee, H. J.; Girshick, S. L.; McMurry, P. H.; Heberlein, J. Hypersonic Plasma Particle Deposition of Nanostructured Silicon and Silicon Carbide. *J. Aerosol Sci.* **1998**, *29*, 707−720.

(16) Holman, Z. C.; Kortshagen, U. R. A Flexible Method for Depositing Dense Nanocrystal Thin Films: Impaction of Gemanium Nanocrystals. *Nanotechnology* **2010**, *21*, 335302.

(17) Niesar, S.; Stegner, A. R.; Pereira, R. N.; Hoeb, M.; Wiggers, H.; Brandt, M. S.; Stutzmann, M. Defect Reduction in Silicon Nanoparticles by Low-Temperature Vacuum Annealing. *Appl. Phys. Lett.* **2010**, *96*, 193112.

(18) Marra, D. C.; Edelberg, E. A.; Naone, R. L.; Aydil, E. S. Silicon Hydride Composition of Plasma-Deposited Hydrogenated Amorphous and Nanocrystalline Silicon Films and Surfaces. *J. Vac. Sci. Technol., A* **1998**, *16*, 3199−3210.

(19) Agarwal, S.; Sriraman, S.; Takano, A.; van de Sanden, M. C. M.; Aydil, E. S.; Maroudas, D. Mechanism and Activation Energy Barrier for H Abstraction by H(D) from a-Si:H Surfaces. *Surf. Sci.* **2002**, *515*, L469−L474.

(20) Manousiadis, P.; Gardelis, S.; Nassiopoulou, A. G. Lateral Electronic Transport in 2D Arrays of Oxidized Si Nanocrystals on Quartz: Columb Blockade Effect and Role of Hydrogen Passivation. *J. Appl. Phys.* **2011**, *109*, 083718.

(21) Pereira, R. N.; Rowe, D. J.; Anthony, R. J.; Kortshagen, U. Oxidation of Freestanding Silicon Nanocrystals Probed with Electron Spin Resonance of Interfacial Dangling Bonds. *Phys. Rev. B* **2011**, *83*, 155327.

(22) Shklovskii, B. I.; Efros, A. L. *Electronic Properties of Doped Semiconductors*; Springer-Verlag: Berlin, 1984; Vol. *1*.

(23) Zhou, X.-L.; Flores, C. R.; White, J. M. Adsorption and Decomposition of Water on Si(100) − A TPD and SSIMS Study. *Appl. Surf. Sci.* **1992**, *62*, 223−237.

(24) Jansson, U.; Uram, K. J. The Adsorption of Hydrogen on Si(111)-7 × 7 as Studied by Multiple-Internal Reflection Spectroscopy. *J. Chem. Phys.* **1989**, *91*, 7978−7987.

(25) Gupta, P.; Dillon, A. C.; Bracker, A. S.; George, S. M. FTIR Studies of H_2O and D_2O Decomposition on Porous Silicon Surfaces. *Surf. Sci.* **1991**, *245*, 360−372.

(26) Han, S. M.; Aydil, E. S. Study of Surface Reactions during Plasma Enhanced Chemical Vapor Deposition of SiO_2 from SiH_4, O_2 and Ar Plasma. *J. Vac. Sci. Technol., A* **1996**, *14*, 2062−2070.

(27) Winters, B. J.; Holm, J.; Roberts, J. T. Thermal Processng and Native Oxidation of Silicon Nanoparticles. *J. Nanopart. Res.* **2011**, *13*, 5473−5484.

(28) Ubara, H.; Imura, T.; Hiraki, A. Formation of Si-H Bonds on the Surface of Microcrystalline Silicon Covered with SiO_x by HF Treatment. *Solid State Commun.* **1984**, *50*, 673−675.

(29) Zhou, Z. H.; Aydil, E. S.; Gottscho, R. A.; Chabal, Y. J.; Reif, R. Real-Time In Situ Monitoring of Room-Temperature Silicon Surface Cleaning Using Hydrogen and Ammonia Plasmas. *J. Electrochem. Soc.* **1993**, *140*, 3316−3321.
(30) Salace, G.; Hadjadj, A.; Petit, C.; Jourdain, M. Temperature Dependance of the Electron Affinity Difference Between Si and SiO_2 in Polysilicon ($n^{(+)}$)-Oxide-Silicon (p) Structures: Effect of the Oxide Thickness. *J. Appl. Phys.* **1999**, *85*, 7768−7773.
(31) Traversa, E. Ceramic Sensors for Humidity Detection − The State-of-the-Art and Future Developments. *Sens. Actuators, B* **1995**, *23*, 135−156.
(32) Mares, J. J.; Kristofik, J.; Hulicius, E. Influence of Humidity on Transport in Porous Silicon. *Thin Solid Films* **1995**, *255*, 272−275.
(33) Parks, G. A.; Anderson, J. H. Electrical Conductivity of Silica Gel in the Presence of Adsorbed Water. *J. Phys. Chem.* **1968**, *72*, 3662−3668.
(34) Dubey, G.; Lopinski, G. P.; Rosei, F. Influence of Physisorbed Water on the Conductivity of Hydrogen Terminated Silicon-on-Insulator Surfaces. *Appl. Phys. Lett.* **2007**, *91*, 232111.
(35) Dubey, G.; Rosei, F.; Lopinski, G. P. Molecular Modulatiomn of Condutivity on H-Terminated Silicon-on-Insulator Substrates. *Small* **2010**, *6*, 2892−2899.